NANOSYSTEMS:
PHYSICS, CHEMISTRY, MATHEMATICS

Original article

Osminina A.A., et al. *Nanosystems: Phys. Chem. Math.*, 2025, **16** (4), 472–482.
http://nanojournal.ifmo.ru
DOI 10.17586/2220-8054-2025-16-4-472-482

Phase formation in the $BiPO_4$–YPO_4–(H_2O) system

Alena A. Osminina[1,2,3,a], Dmitry P. Elovikov[1,4,b], Olga V. Proskurina[2,3,c]

[1]Branch of Petersburg Nuclear Physics Institute named by B. P. Konstantinov of National Research Centre "Kurchatov Institute" – Institute of Silicate Chemistry, St. Petersburg, Russia

[2]Ioffe Institute, St. Petersburg, Russia

[3]St. Petersburg State Institute of Technology, St. Petersburg, Russia

[4]St. Petersburg Electrotechnical University "LETI", St. Petersburg, Russia

[a]alenaosminina3001@gmail.com, [b]syncdima@mail.ru, [c]proskurinaov@mail.ru

Corresponding author: Alena A. Osminina, alenaosminina3001@gmail.com

ABSTRACT This work is devoted to the study of phase equilibria in the $BiPO_4$–YPO_4–(nH_2O) system under mild conditions. It was shown that using the precipitation method leads to crystallization of the samples into the rhabdophane phase $YPO_4 \cdot nH_2O$ and the ximengite phase $BiPO_4$. Hydrothermal treatment of the samples at 160 °C results in the gradual transformation of hexagonal yttrium phosphate with a rhabdophane-type structure into tetragonal xenotime YPO_4, and hexagonal bismuth phosphate with a ximengite-type structure into monoclinic bismuth phosphate (space group $P2_1/n$). The transformation into the stable phases of xenotime and monoclinic bismuth phosphate is almost complete after 28 days of isothermal holding under hydrothermal conditions at 160 °C. Moreover, the lower the content of the second component in samples containing both Bi and Y, the faster the structural transformation into the stable phase proceeds. A solid solution based on monoclinic bismuth phosphate with the composition $Bi_{0.94}Y_{0.06}PO_4$ is formed in the system. Before disappearing, the rhabdophane-type phase represents a solid solution with the composition $Y_{0.8}Bi_{0.2}PO_4 \cdot nH_2O$. The crystallite sizes of all phases increase with an increase in the bismuth content in the system.

KEYWORDS nanocrystals, phase formation, bismuth phosphate, yttrium orthophosphate, hydrothermal synthesis

ACKNOWLEDGEMENTS The authors are grateful to Corresponding Member of the Russian Academy of Sciences V. V. Gusarov for his attention to the work and valuable comments, as well as D. P. Danilovich for his help in conducting the research. The work of A. A. O. and D. P. E. was carried out with the support of the Russian Science Foundation project No. 24-13-00445. Scanning electron microscopy and elemental analyses of samples were performed employing the equipment of the Engineering Center of the St. Petersburg State Institute of Technology. X-ray diffraction studies were carried out using the DRON-8 diffractometer in the laboratory of new inorganic materials (Ioffe Institute).

FOR CITATION Osminina A.A., Elovikov D.P., Proskurina O.V. Phase formation in the $BiPO_4$–YPO_4–(H_2O) system. *Nanosystems: Phys. Chem. Math.*, 2025, **16** (4), 472–482.

1. Introduction

At present, compounds of the type $Me_{III}PO_4$ and complex orthophosphates of trivalent cations are considered promising functional materials due to their nonlinear optical properties and applications in the production of catalysts, ceramic dielectric materials, fluorescent materials, fuel cells, and detergent components [1–3]. Rare-earth element (REE) orthophosphates are of particular interest owing to their high melting points ($T_m \approx 1900$ – 2300 °C), low solubility in aggressive media, and high isomorphic capacity [4–11]. Materials based on REE orthophosphates are considered promising candidates as matrices for immobilizing toxic and radioactive elements and as heat-resistant ceramics [12]. Luminescent nanomaterials based on doped REE orthophosphates have potential applications in optical systems, high-definition displays, medical and biological analysis, fluorescent imaging, drug delivery, and biomolecule detection [13]. The incorporation of Bi^{3+} ions into the crystal lattice of yttrium orthophosphate has a favorable effect on its luminescence intensity [14]. As a result, bismuth-doped nanocrystalline yttrium orthophosphates have found applications as optical amplifiers, light-emitting devices, displays, and low-threshold lasers [15].

Depending on the synthesis methods and conditions, REE orthophosphates can be obtained in various structural modifications: monazite with space group $P2_1/n$ and xenotime with space group $I4_1/amd$. At low temperatures, REE orthophosphates can also crystallize in the structures of rhabdophane ($P6_222$, or $C2$, or $P3_121$) [16–18] and churchite ($C2/c$), both containing structural water. An increase in temperature leads to the transformation of hydrated compounds

into anhydrous phases [10,19,20]. Doping REE orthophosphates with various elements results in the formation of different phases within the system [13, 21–23].

Bismuth phosphate $BiPO_4$ exists in several crystalline modifications: a hexagonal phase with a ximingite-type structure ($P3_121$) and two monoclinic phases – a low-temperature phase ($P2_1/n$) and a high-temperature phase ($P2_1/m$) [24–26].

It is also known that bismuth phosphate $BiPO_4$ finds particular application in catalysis [27, 28], ion probing [29], and the separation of radioactive elements [30, 31], as well as in the enhancement of the electrical properties of phosphate glasses [32, 33]. Recently, photoluminescent properties of bismuth phosphate $BiPO_4$ have been identified [34].

Due to the relatively small difference in the ionic radii of Bi^{3+} and REE ions, bismuth phosphate can be doped with rare-earth element ions [35]. REE-doped $BiPO_4$ nanoparticles are promising candidates for photonic and luminescent applications.

Promising methods for the production of nanoparticles include low-temperature synthesis techniques for solid-state materials [36–39], including "soft chemistry" methods [40]. Typically, the reaction medium in low-temperature synthesis of oxide nanocrystals consists of aqueous solutions and aqueous dispersions of various compositions [41], which introduces certain challenges in obtaining nanoparticles based on anhydrous oxide phases with a specified structure [42, 43].

Currently, several methods for the synthesis of single-phase micro- and nanoparticles of $BiPO_4$ are known. Nanorods of the hexagonal phase of $BiPO_4$ were obtained using a sonochemical method without the use of surfactants/ligands at room temperature [44]. It is noted that under hydrothermal synthesis conditions at 160 °C, a phase transformation from the hexagonal phase h-$BiPO_4$ to the low-temperature monoclinic phase m-$BiPO_4$ occurs, accompanied by a morphological transformation from nanorods to monoclinic microcrystals [45].

For the synthesis of nanocrystalline REE orthophosphates, "soft chemistry" methods are commonly used, including co-precipitation [46, 47] and hydrothermal methods [48, 49]. Sometimes, the precipitates obtained by "soft chemistry" methods are annealed at $T \geq 800$ °C to obtain anhydrous samples [16], or are initially subjected to high-temperature sintering [22, 23].

The phase diagram of the $BiPO_4$–YPO_4 system is not presented in the literature.

The work is aimed at studying the mutual influence of the components in the $BiPO_4$–YPO_4–(nH_2O) system on phase formation using "soft chemistry" methods, including precipitation and hydrothermal treatment.

2. Material sand methods

For the synthesis of nanocrystalline powders with the overall composition $Y_{1-x}Bi_xPO_4$ ($0 \leq x \leq 1$), the starting reagents used were bismuth nitrate $Bi(NO_3)_3 \cdot 5H_2O$ (analytical grade), yttrium nitrate $Y(NO_3)_3 \cdot 6H_2O$(technical grade), 6 M nitric acid (technical grade), and ammonium dihydrogen phosphate $(NH_4)_2HPO_4$ (analytical grade).

To precipitate the orthophosphates, a 0.1 M solution of bismuth nitrate $Bi(NO_3)_3$ was first prepared. To prevent the precipitation of bismuth hydroxide, 6 M HNO_3 was added. While continuously stirring, a 0.1 M aqueous solution of yttrium nitrate $Y(NO_3)_3$ was added dropwise to the bismuth nitrate solution in the desired Bi : Y ratio. Then, stoichiometric amounts of a 0.1 M aqueous solution of the precipitant $(NH_4)_2HPO_4$ were added while stirring. The resulting suspensions with pH = 1 were stirred for 30 minutes using a magnetic stirrer at $T = 25$ °C.

The hydrothermal treatment was carried out as follows: the suspension obtained by the precipitation method was placed in a stainless steel autoclave with a Teflon liner (filling ratio 0.85, $P \approx 10$ MPa) and hydrothermally treated at $T = 160$ °C with isothermal holding durations of 9 hours, 9 days, and 28 days.

All obtained samples were washed with distilled water until pH = 7, precipitated by centrifugation (3500 rpm), dried at $T = 80$ °C for 15 hours, and ground in an agate mortar.

To study the particle morphology and determine the composition of the samples, X-ray spectroscopic microanalysis (XPS) was performed using a Tescan Vega 3 SBH scanning electron microscope (Tescan, Czech Republic) equipped with an Oxford Instruments INCA x-act attachment (Oxford Instruments, UK). Due to the overlap of the energy spectra of the $K\alpha$-series of phosphorus (2.013 keV) and the $L\alpha$-series of yttrium (1.922 keV), the yttrium content in the system was determined using the $K\alpha$-series of yttrium (14.955 keV). Measurements were taken in the range up to 20 keV across three different areas, averaging the obtained values.

X-ray diffraction (XRD) analysis of the samples was performed using powder diffraction patterns obtained with a DRON-8N X-ray diffractometer (Bourevestnik, Russia) equipped with a copper anode X-ray tube (Kα doublet), in the angular range of 2θ = 10 – 70° with a step size of 0.0142°. Qualitative analysis of the samples was carried out using the ICSD PDF-2 database. The unit cell parameters of all phases were determined by recording diffraction patterns of samples mixed with NaCl, calibrated using the internal standard method with the powder XRD standard Si640f (NIST, USA). Full-profile phase analysis was performed using the Rietveld method with the PDWin and SmartLab Studio II v4.4.241.0 software suite (Rigaku Corporation, Japan). The phase fractions, determined by the Rietveld method and expressed in mass percentages, were converted to mole percentages. For this conversion, it was assumed that the phase with the rhabdophane structure contains 0.667 moles of water per formula unit [49]. The average crystallite size was determined using the Scherrer equation from the non-overlapping reflections of each phase

3. Results and discussion

According to the elemental analysis data, the molar ratio (Bi + Y) : P is close to 1:1 in all samples, which corresponds to the stoichiometry of the orthophosphate. For further designation of the samples, the relative molar fraction of bismuth with respect to the sum of bismuth and yttrium in the samples is used: for the nominal composition, the notation "Bix" is used, where $x = n(\mathrm{Bi})/(n(\mathrm{Bi}) + n(\mathrm{Y}))$, with n(Bi) and n(Y) being the molar fractions of bismuth and yttrium in the sample as synthesized; for the samples obtained by the precipitation method and subjected to hydrothermal treatment for different durations, the notation "Bi$x(\tau)$" is used, where n(Bi) and n(Y) are the molar fractions of bismuth and yttrium in the sample determined by X-ray spectroscopic microanalysis (XPS), and τ is the duration of the isothermal treatment under hydrothermal conditions. The samples obtained by the precipitation method are designated as "Bix (init.)". The nominal composition and results of elemental analysis are presented in the Table 1.

TABLE 1. Sample designation according to the nominal composition, bulk composition based on X-ray spectroscopic microanalysis (XPS) data, and the duration of hydrothermal treatment

Designation of samples				
Nominal composition, x, mol. frac.	Gross composition, $x(\tau)$, mol. frac.			
	Precipitation	Duration of hydrothermal treatment at 160 °C		
		9 hours	9 days	28 days
Bi0.00	Bi0.00(init.)	Bi0.00(9 h.)	Bi0.00(9 d.)	Bi0.00(28 d.)
Bi0.05	Bi0.13(init.)	Bi0.04(9 h.), Bi0.06(9 h.)*	Bi0.06(9d.)	—
Bi0.07	—	Bi0.07(9 h.)	—	—
Bi0.10	Bi0.34(init.)	—	—	Bi0.11(28 d.)
Bi0.20	—	Bi0.19(9 h.)	Bi0.15(9d.)	—
Bi0.30	Bi0.59(init.), Bi0.84(init.)*	Bi0.35(9 h.)	Bi0.34(9d.)	Bi0.23(28 d.)
Bi0.40	—	Bi0.60(9 h.)	—	—
Bi0.50	Bi0.93(init.)	—	Bi0.54(9d.)	Bi0.56(28 d.)
Bi0.60	—	Bi0.76(9h.)	Bi0.64(9d.)	—
Bi0.70	—	Bi0.87(9 h.)	Bi0.74(9d.)	Bi0.68(28 d.)
Bi0.80	—	Bi0.92(9 h.)	Bi0.84(9d.)	—
Bi0.90	Bi0.97(init.)	Bi0.95(9 h.)	Bi0.93(9d.)	Bi0.94(28 d.)
Bi1.00	Bi1.00(init.)	Bi1.00(9 h.)	Bi1.00(9d.)	Bi1.00(28 d.)

*The samples were obtained with different degrees of washing of the precipitate.

According to the elemental analysis data for the samples (Table 1) obtained both by the precipitation method and hydrothermal treatment, the experimentally determined composition of the samples contains less yttrium compared to the nominal composition. This may be due to the washing out of nanocrystalline yttrium orthophosphate during the washing process of the samples. According to study [49], the crystallite size of yttrium orthophosphate with a xenotime structure can be around 4 – 10 nm, which significantly complicates its separation during centrifugation and leads to its removal with the washing water. The sample Bi0.59(init.) was obtained by a single washing of the precipitate with a nominal composition of Bi0.30, while the sample Bi0.84(init.) was obtained by applying a three-step washing of the precipitate.

According to the X-ray diffraction data for the $BiPO_4$–YPO_4–(nH_2O) system samples obtained by the precipitation method (Fig. A1 in Appendix), the Bi0.00(init.) sample exhibits broadened reflections corresponding to the xenotime

structure (PDF-2 Card 00-011-0254). Samples with compositions ranging from Bi0.13(init.) to Bi0.97(init.) crystallize into the rhabdophane (PDF-2 Card 00-042-0082) and ximengite (PDF-2 Card 00-045-1370) structures. In the Bi1.00(init.) sample, only reflections corresponding to the phase with the ximengite structure are observed.

After hydrothermal treatment at 160 °C with an isothermal holding time of 9 hours (Fig.A2 in Appendix), the samples crystallize into phases with xenotime, rhabdophane, ximengite, and low-temperature monoclinic bismuth phosphate structures. According to the X-ray diffraction data, the Bi1.00(9 h.) sample consists of the low-temperature monoclinic phase of $BiPO_4$ (PDF-2 Card 00-015-0767), while the Bi0.00(9 h.) sample crystallizes in the tetragonal xenotime-type structure of YPO_4 (for all isothermal holding times under hydrothermal conditions). In the samples containing both Bi and Y, the formation of phases with ximengite and rhabdophane structures is observed. The presence of bismuth in the Bi0.04(9 h.) and Bi0.06(9 h.) samples leads to the formation of a tetragonal xenotime-type phase in addition to the rhabdophane phase, whereas the presence of yttrium in the Bi0.95(9 h.) sample promotes the formation of the low-temperature monoclinic bismuth phosphate phase alongside the ximengite structure phase.

An increase in the isothermal holding time under hydrothermal conditions to 9 and 28 days leads to an expansion of the stability range of phases with monoclinic bismuth phosphate and tetragonal yttrium phosphate (xenotime-type) structures. After 9 days of isothermal holding under hydrothermal conditions (Fig. A3 in Appendix), in samples containing both Bi and Y, the formation of tetragonal YPO_4 is observed in compositions from Bi0.06(9 d.) to Bi0.64(9 d.), while the monoclinic bismuth phosphate phase is formed in samples Bi0.15(9 d.) and from Bi0.54(9 d.) to Bi0.93(9 d.).

After 28 days of isothermal holding under hydrothermal conditions (Fig. A4 in Appendix), the formation of the xenotime phase is observed in samples from Bi0.11(28 d.) to Bi0.68(28 d.), while the formation of the monoclinic bismuth phosphate phase is observed from Bi0.11(28 d.) to Bi0.94(28 d.).

In the samples obtained by the precipitation method with compositions from Bi0.13(init.) to Bi0.97(init.), the unit cell volumes of the two coexisting phases – $YPO_4 \cdot nH_2O$ with the rhabdophane structure and $BiPO_4$ with the ximengite structure – remain constant, which may indicate the absence of solid solution formation based on these phases (Fig. 1a).

Hydrothermal synthesis with an isothermal holding time of 9 hours (Fig. 1b) also leads to the formation of two phases in the samples from Bi0.07(9 h.) to Bi0.92(9 h.). These samples contain a $BiPO_4$ phase with the ximengite structure and a $YPO_4 \cdot nH_2O$ phase with the rhabdophane structure, exhibiting constant V/Z values across the specified composition range, which indicates the absence of solid solution formation. The Bi0.04(9 h.) and Bi0.06(9 h.) samples are three-phase and crystallize into phases corresponding to $BiPO_4$ with the ximengite structure, $YPO_4 \cdot nH_2O$ with the rhabdophane structure, and YPO_4 with the xenotime structure. The Bi0.95(9 h.) sample is also three-phase, crystallizing into $BiPO_4$ phases with ximengite and monoclinic bismuth phosphate structures, as well as a $YPO_4 \cdot nH_2O$ phase with the rhabdophane structure.

With an increase in the isothermal holding time to 9 days (Fig. 1c), a gradual transformation of hexagonal yttrium phosphate with the rhabdophane structure into tetragonal yttrium phosphate with the xenotime structure, as well as hexagonal bismuth phosphate with the ximengite structure into monoclinic bismuth phosphate, occurs. Three-phase regions are observed for samples with compositions from Bi0.15(9 d.) to Bi0.84(9 d.). It can be seen that the unit cell volume of the phase with the rhabdophane structure in the samples obtained by precipitation and after 9 hours of hydrothermal treatment, and the unit cell volume of the phase with the ximengite structure in the samples obtained by precipitation and hydrothermal treatment for 9 hours and 9 days, remain constant at approximately $(V/Z)_{\text{rhabd.}} \approx 85$ Å^3 and $(V/Z)_{\text{xim.}} \approx 91$ Å^3, respectively. The unit cell volume $(V/Z)_{\text{rhabd.}}$ after 9 days of hydrothermal treatment increases to ~ 86.5 Å^3, indicating the formation of a solid solution with an approximate composition of $Y_{0.92}Bi_{0.08}PO_4 \cdot nH_2O$, and after 28 days (Fig. 1d) for the $Bi_{0.68}$(28 d.) sample, to ~ 87.5 Å^3, corresponding to the formation of a solid solution with the composition $Y_{0.8}Bi_{0.2}PO_4 \cdot nH_2O$. The unit cell volume of xenotime remains constant for all compositions and hydrothermal treatment durations ($(V/Z)_{\text{xen}} \approx 72$ Å^3). The unit cell volume (V/Z) of the monoclinic $BiPO_4$ phase in the Bi0.95(9 h.) and Bi1.00(9 h.) samples after 9 hours of hydrothermal treatment is also constant at ~ 74 Å^3. However, after 9 and 28 days of hydrothermal treatment, for samples containing Y, a decrease in the unit cell volume of the monoclinic $BiPO_4$ phase to ~ 73 Å^3 is observed, which may indicate the formation of a solid solution with the composition $Bi_{0.94}Y_{0.06}PO_4$.

The absence of data in Fig. 2 for the rhabdophane structure in the Bi0.97(init.), Bi0.95(9 h.), and Bi0.93(9 d.) samples is due to the low content of this phase (less than 2 mol.%), which makes it impossible to accurately determine the unit cell parameters.

The phase composition analysis by the Rietveld method (Fig. 2a) for the $BiPO_4$–YPO_4–(nH_2O) system samples obtained by the precipitation method shows the presence of a xenotime phase in the Bi0.00(init.) sample and a ximengite phase in the Bi1.00(init.) sample. Samples containing both Bi and Y crystallize in phases with rhabdophane $YPO_4 \cdot nH_2O$ and ximengite $BiPO_4$ structures in molar ratios close to the elemental composition of the samples.

For the samples obtained with an isothermal holding time of 9 hours (Fig. 2b), the transformation of hexagonal ximengite into monoclinic bismuth phosphate is observed in the Bi0.95(9 h.) sample. A phase transition from hexagonal rhabdophane to tetragonal xenotime is also observed in the samples with low bismuth content. With an increase in the total bismuth content in the samples, there is a corresponding decrease in the proportion of the rhabdophane $YPO_4 \cdot nH_2O$ phase and an increase in the proportion of the phase with the ximengite structure.

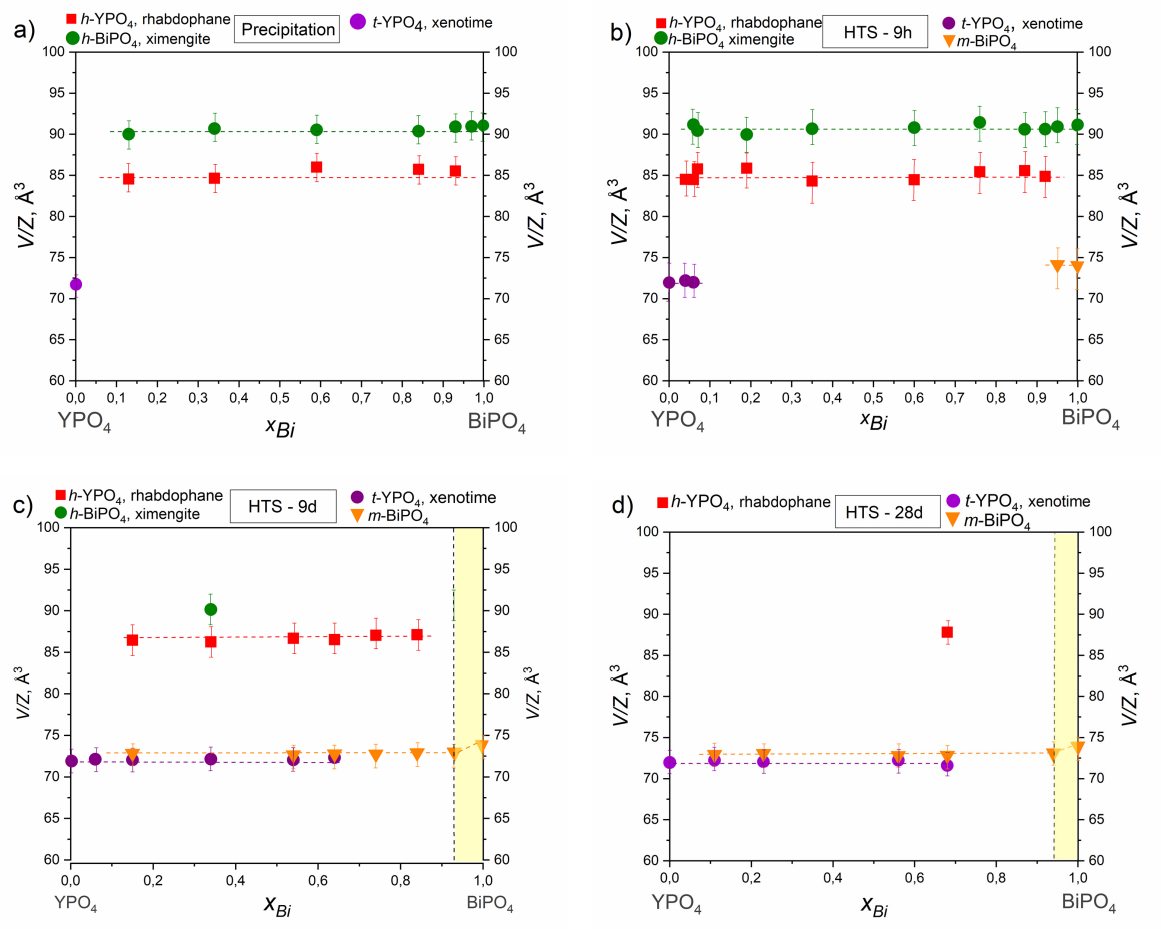

FIG. 1. Dependence of the unit cell volumes of different phases, normalized to the number of formula units per unit cell, on the total actual bismuth content in samples obtained by the methods: a) precipitation, b) hydrothermal treatment for 9 hours, c) hydrothermal treatment for 9 days, d) hydrothermal treatment for 28 days. The solid solution formation region based on monoclinic $BiPO_4$ is highlighted in color

An increase in the duration of the isothermal holding time under hydrothermal conditions to 9 days (Fig. 2c) leads to the expansion of the concentration range for the formation of more stable phases – monoclinic bismuth phosphate and tetragonal yttrium phosphate with the xenotime structure – as well as to a decrease in the amounts of metastable phases with the structures of rhabdophane $Y_{0.92}Bi_{0.08}PO_4 \cdot nH_2O$ and ximengite $BiPO_4$.

In the case of hydrothermal treatment with an isothermal holding time of 28 days (Fig. 2d), the system for almost all compositions reaches a state of two-phase equilibrium based on the stable phases at 160 °C with xenotime (YPO_4) and monoclinic $BiPO_4$ structures. Only in the sample Bi0.68(28 d.) is the presence of $\sim$ 6 mol.% of a rhabdophane-structured phase with the composition $Y_{0.8}Bi_{0.2}PO_4 \cdot nH_2O$ observed.

For the samples obtained by the precipitation method, from Bi0.13(init.) to Bi0.93(init.), an increase in the average crystallite sizes of the phases with rhabdophane and ximengite structures from approximately 10 to 40 nm is observed with increasing bismuth content in the system (Fig. 3a). Moreover, the crystallite sizes of these two phases are almost identical. Further increase in the bismuth content (up to the Bi1.00(init.) sample) leads to an increase in the average crystallite size of the ximengite-structured phase to $\sim$ 70 nm. The average crystallite size of the xenotime-structured phase in the Bi0.00(init.) sample is $\sim$ 3 – 5 nm.

For the samples obtained by hydrothermal synthesis with an isothermal holding time of 9 hours, from Bi0.04(9 h.) to Bi0.60(9 h.), an increase in the bismuth molar fraction in the system leads to a slight increase in the average crystallite sizes of the phases with rhabdophane and ximengite structures from $\sim$ 45 to 48 nm (Fig. 3b). Further increase in the bismuth content up to Bi0.92(9 h.) results in an increase in the average crystallite sizes of the phases with rhabdophane and ximengite structures to $\sim$ 50 nm and 63 nm, respectively. The average crystallite sizes of the monoclinic bismuth phosphate phase are $\sim$ 85 nm, and the average crystallite size of the xenotime-structured phase is $\sim$ 35 nm.

With an increase in the isothermal holding time under hydrothermal conditions to 9 days (Fig. 3c), growth in the crystallite sizes of xenotime is observed from $\sim$ 40 nm to $\sim$ 55 nm for samples from Bi0.00(9 d.) to Bi0.64(9 d.). The

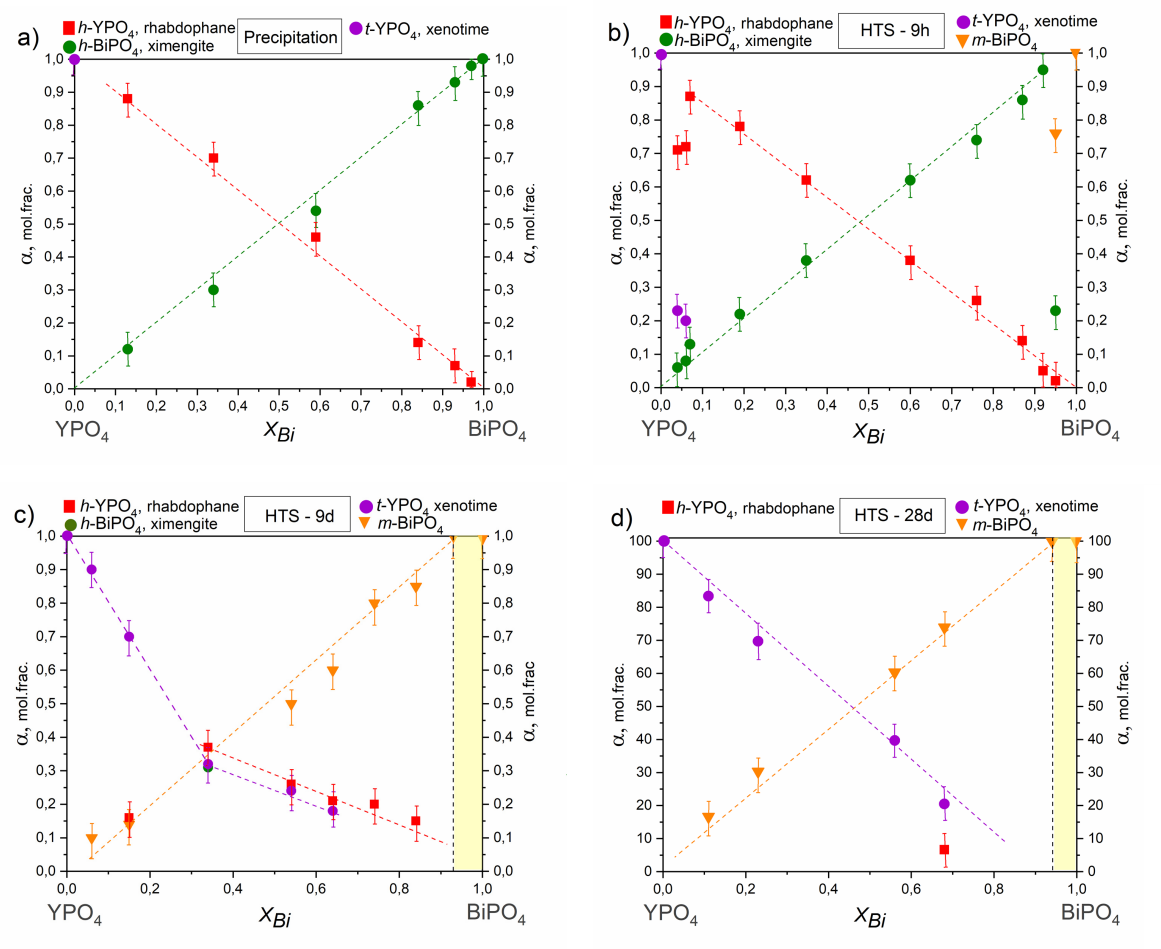

FIG. 2. Phase content (α, mol.%) in the $BiPO_4$–YPO_4–(H_2O) system as a function of the total actual bismuth content in samples obtained by the methods: a) precipitation, b) hydrothermal treatment for 9 hours, c) hydrothermal treatment for 9 days, d) hydrothermal treatment for 28 days. The single-phase region of compositions is highlighted in color

crystallite sizes of the hexagonal yttrium phosphate with a rhabdophane structure increase from $\sim$ 35 nm to $\sim$ 70 nm for compositions from Bi0.15(9 d.) to Bi0.84(9 d.). For the hexagonal bismuth phosphate with a ximengite structure, crystallite growth from $\sim$ 45 nm to $\sim$ 78 nm is observed for samples from Bi0.34(9 d.) to Bi0.93(9 d.). Crystallite growth of the monoclinic bismuth phosphate phase from $\sim$ 52 nm to $\sim$ 85 nm is observed in samples from Bi0.15(9 d.) to Bi1.00(9 d.).

An increase in the isothermal holding time under hydrothermal conditions to 28 days (Fig. 3d) does not lead to a significant change in the average crystallite sizes of the phases with the xenotime structure YPO_4 and the monoclinic $BiPO_4$ structure compared to the samples obtained after 9 days of isothermal treatment.

Analysis of SEM micrographs (Fig. 4) of the synthesized samples obtained by precipitation and hydrothermal synthesis methods shows that yttrium phosphate crystallizing in the xenotime structure forms aggregates composed of YPO_4 particles, whose sizes are nearly identical to the crystallite sizes of the YPO_4 phase ($\sim$ 5 to $\sim$ 40 nm), as observed in work [49]. Bismuth phosphate particles obtained by the precipitation method appear as aggregates of small rounded particles corresponding to the phase with the xenotime-type structure, with particle sizes of approximately 200 – 300 nm. Under hydrothermal conditions, bismuth phosphate crystallizes in the form of large monoclinic crystals with sizes ranging from $\sim$ 0.5 to 2 μm. For the samples containing both Bi and Y, the formation of rod-like particles corresponding to the hexagonal phase of yttrium phosphate$YPO_4 \cdot nH_2O$ with the rhabdophane structure is observed.

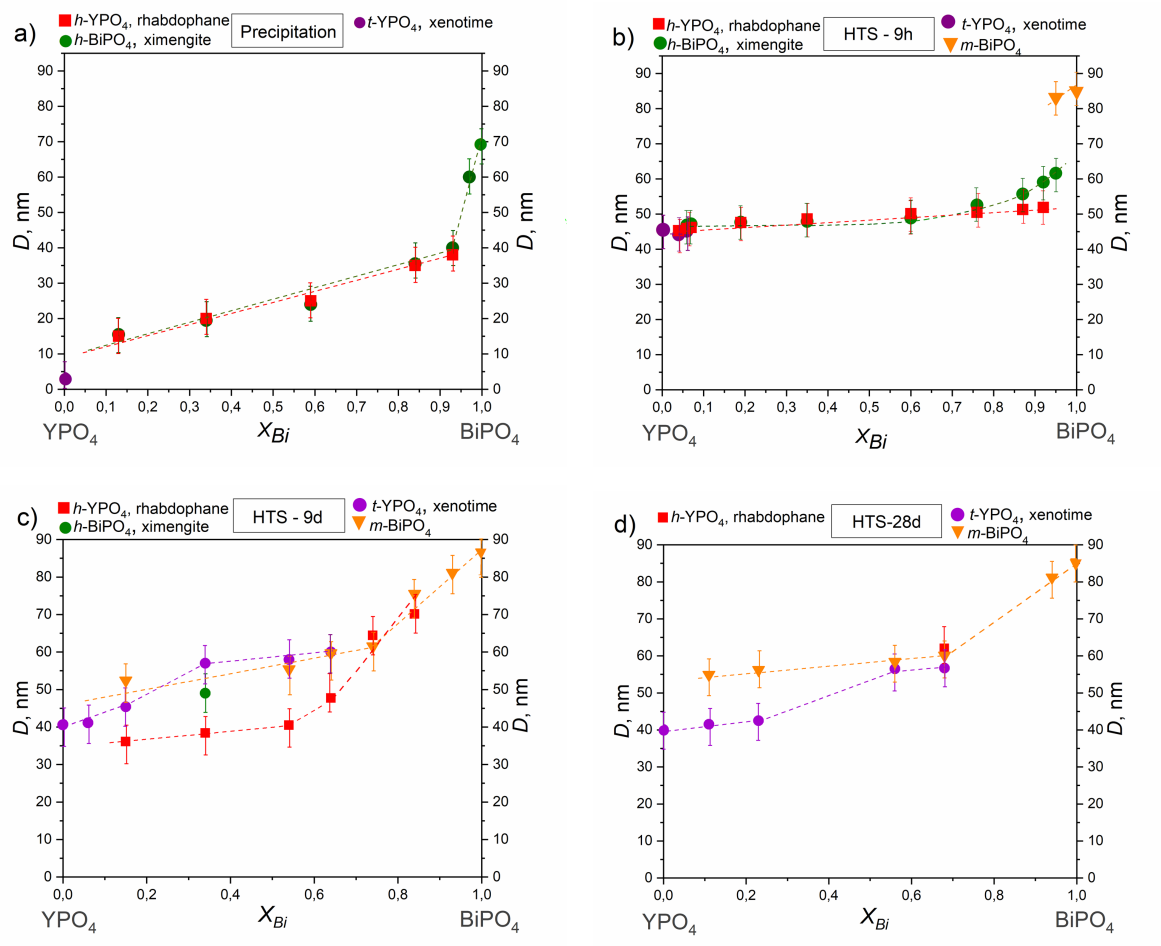

FIG. 3. Crystallite sizes of all phases as a function of the total actual bismuth content in samples obtained by the methods: a) precipitation, b) hydrothermal treatment for 9 hours, c) hydrothermal treatment for 9 days, d) hydrothermal treatment for 28 days

4. Conclusion

It is shown that in the $BiPO_4$–YPO_4–(nH_2O) system, using the precipitation method, samples with compositions ranging from $x = 0.13$ to $x = 0.97$ crystallize in two phases, namely the rhabdophane and xenotime structures. Hydrothermal treatment at 160 °C leads to the gradual transformation of hexagonal bismuth phosphate with a ximengite structure into a low-temperature monoclinic bismuth phosphate, and hexagonal yttrium phosphate with a rhabdophane structure into tetragonal xenotime. Increasing the duration of isothermal treatment to 9 days promotes the formation of solid solutions based on monoclinic bismuth phosphate $Bi_{0.94}Y_{0.06}PO_4$ and hexagonal yttrium phosphate $Y_{0.92}Bi_{0.08}PO_4 \cdot nH_2O$ with a rhabdophane structure.

Samples obtained via hydrothermal synthesis with a 28-day isothermal treatment are two-phased and contain stable phases of xenotime and monoclinic bismuth phosphate across the entire composition range, except for the sample with a bismuth content of $x = 0.68$, in which 6 mol.% of a solid solution phase with the structure of rhabdophane, composition $Y_{0.8}Bi_{0.2}PO_4 \cdot nH_2O$, is present. A solid solution is formed based on the thermodynamically stable monoclinic bismuth phosphate phase with the composition $Bi_{0.94}Y_{0.06}PO_4$. The lower the content of the second component in samples containing both Bi and Y, the faster the structural transformation into the stable phase occurs.

An increase in the molar fraction of bismuth for samples obtained by the precipitation method leads to an increase in the average crystallite sizes of all phases from $\sim$ 10 to 70 nm. For samples obtained by hydrothermal synthesis, an increase in the average crystallite sizes is observed with the rise in bismuth content in the system and with an increase in the duration of isothermal treatment.

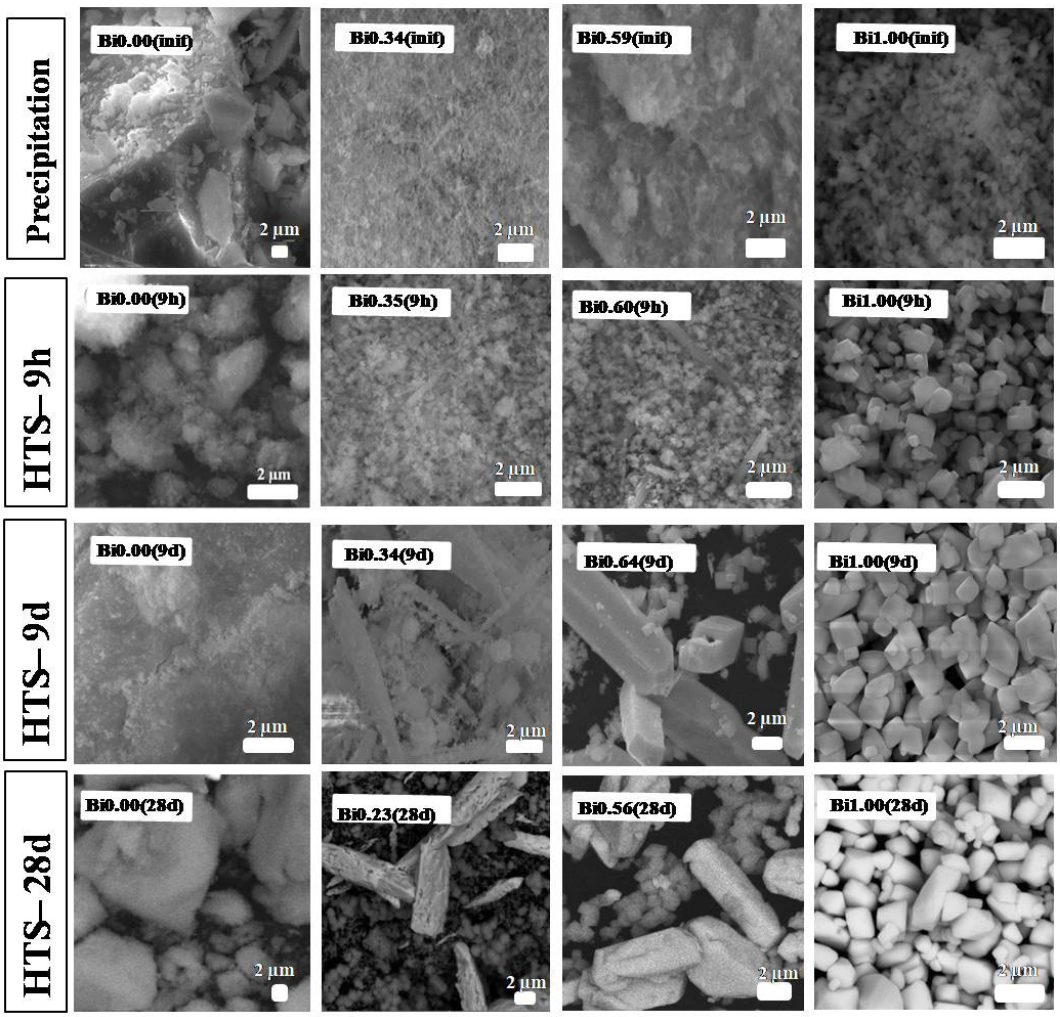

FIG. 4. Microphotographs of samples obtained by precipitation and hydrothermal synthesis methods

Appendix

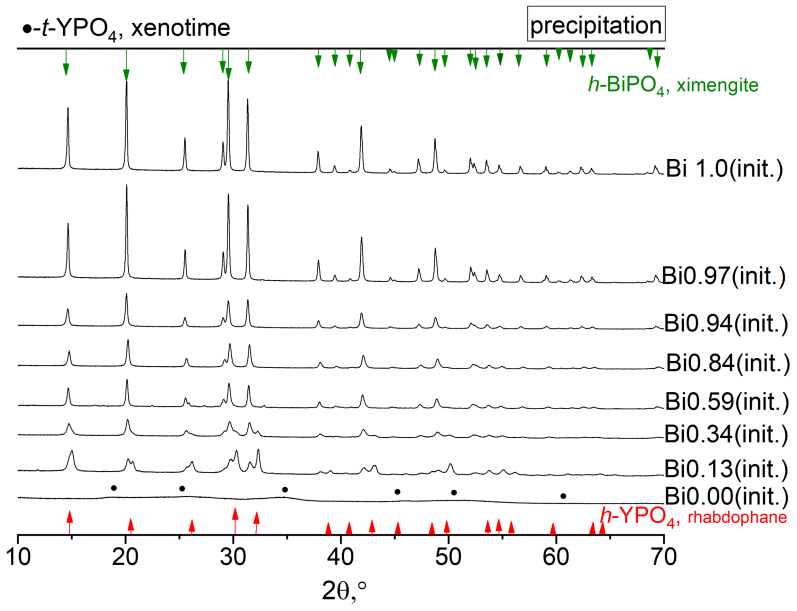

FIG. A1. X-ray diffraction patterns of samples obtained by the precipitation method

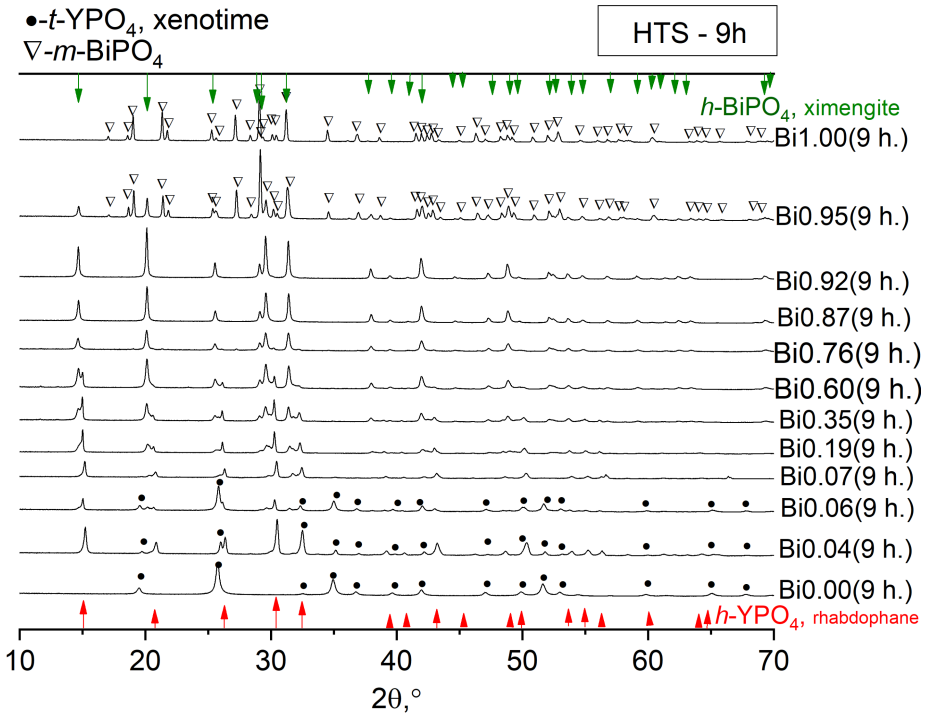

FIG. A2. X-ray diffraction patterns of samples obtained by hydrothermal treatment at 160 °C for 9 hours

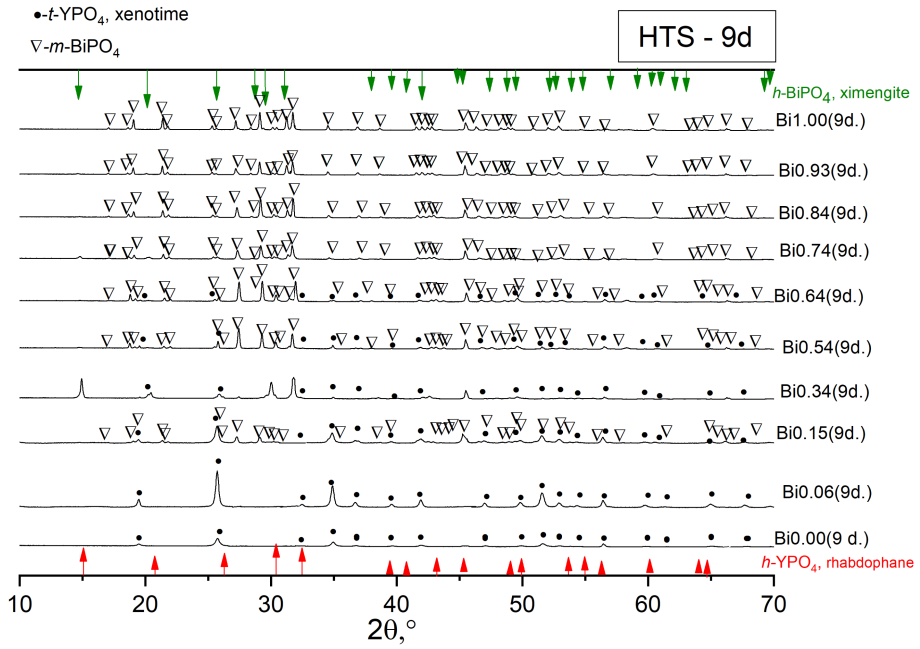

FIG. A3. X-ray diffraction patterns of samples obtained by hydrothermal treatment at 160 °C for 9 days

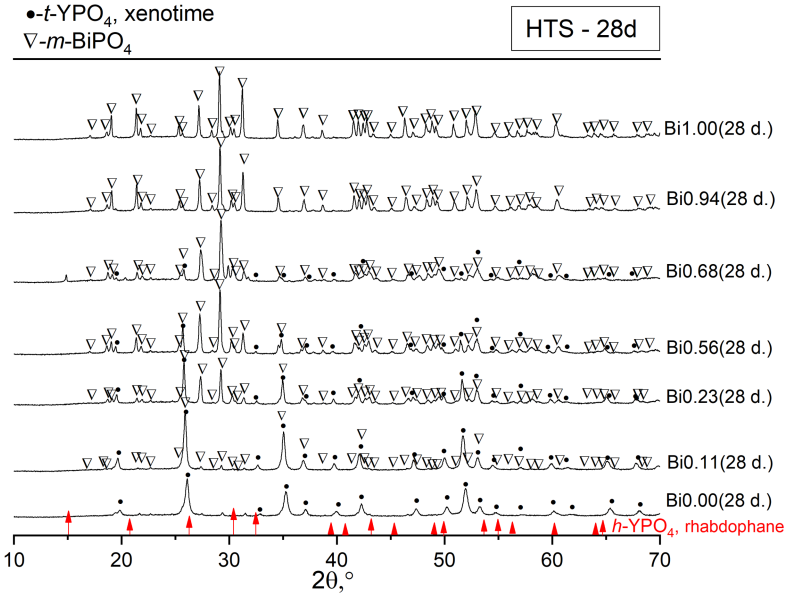

FIG. A4. X-ray diffraction patterns of samples obtained by hydrothermal treatment at 160 °C for 28 days

References

[1] Sankar S., RajA.N., Jyothi C.K., Warrier K.G.K., Padmanabhan P.V.A. Room temperature synthesis of high temperature stable lanthanum phosphate-yttria nanocomposite. *Materials Research Bulletin*, 2012, **47** (7), P. 1835–1837.

[2] Du Foude Kerdaniel E., Clavier N., Dacheux N., Terra O., Podor R.Actinide solubility-controlling phases during the dissolution of phosphate ceramics. *J. Nucl. Mater.*, 2007, **362** (2–3), P. 451–458.

[3] Sroor F.M.A., Edelmannand F.T. *The Rare Earth Elements: Fundamentals and Applications*. Ed. Atwood D.A. Chichester: John Wiley & Sons Ltd, 2012, P. 313–320.

[4] Hikichi Y., Nomura T. Melting Temperatures of Monazite and Xenotime. *J. Am. Ceram. Soc.*, 1987, **70** (10), P. 252.

[5] Horváth I., Bondar I.A., Mezentseva L.P. Thermochemistry of Hydrated Rare Earth Orthophosphates. *J. Therm. Anal.*, 1988, **33** (3), P. 755–760.

[6] Gysi A.P., Williams-Jones A.E., Harlov D. The Solubility of Xenotime-(Y) and Other HREE Phosphates ($DyPO_4$, $ErPO_4$ and $YbPO_4$) in Aqueous Solutions from 100 to 250 °C and Psat. *Chem. Geol.*, 2015, **401**, P. 83–95.

[7] Schlenz H., Heuser J.,Neumann A., Schmitz S., Bosbach D. Monazite as a Suitable Actinide Waste Form. *Zeitschrift fur Krist.*, 2013, **228** (3), P. 113–123.

[8] Huittinen N., Arinicheva Y.,Kowalski P.M., Vinograd V.L.,Neumeier S., Bosbach D. Probing Structural Homogeneity of $La_{1-x}Gd_xPO_4$ Monazite-Type Solid Solutions by Combined Spectroscopic and Computational Studies. *J. Nucl. Mater.*, 2017, **486**, P. 148–157.

[9] Enikeeva M.O., Proskurina O.V., Danilovich D.P., Gusarov V.V. Formation of Nanocrystals Based on Equimolar Mixture of Lanthanum and Yttrium Orthophosphates under Microvawe-Assisted Hydrothermal Synthesis. *Nanosyst.: Phys. Chem. Math.*, 2020, **11** (6), P. 705–715.

[10] Maslennikova T.P., Osipov A.V., Mezentseva L.P., Drozdova I.A., Kuchaeva S.K., Ugolkov V.L., Gusarov V.V. Synthesis, Mutual Solubility, and Thermal Behavior of Nanocrystals in the $LaPO_4$-YPO_4-H_2O System. *Glas. Phys. Chem.*, 2010, **36** (3), P. 351–357.

[11] Enikeeva M.O., Proskurina O.V., Levin A.A., Smirnov A.V., Nevedomskiy V.N., Gusarov V.V. Structure of $Y_{0.75}La_{0.25}PO_4 \cdot 0.67H_2O$ Rhabdophane Nanoparticles Synthesized by the Hydrothermal Microwave Method. *J. Solid State Chem.*, 2023, **319**, 123829.

[12] Enikeeva M.O., Proskurina O.V., Motaylo E.S., Danilovich D.P.,Gusarov V.V. The Influence of Condition of the Monazite Structured $La_{0.9}Y_{0.1}PO_4$ Nanocrystals Sintering on Thermal and Mechanical Properties of the Material. *Nanosyst: Phys. Chem. Math.*, 2021, **12** (6), P. 799–807.

[13] Jinxiu W., Mei L., Huiling J.,Zhaogang L., Hengjun J.,Zhongzhi W. Morphology formation mechanism and fluorescence properties of nano-phosphor YPO_4:Sm^{3+} excited by near-ultraviolet light. *J. Alloys Compd.*, 2019, **821**, 153535.

[14] Khan S.A., Jalil A., Khan Q.U., Irfan R.M., Mehmood I.,Khan K., Kiani M., Dong B., Khan N., Yu J.L., Zhu L., Agathopoulos S. New physical insight into crystal structure, luminescence and optical properties of YPO_4:Dy^{3+}\$Eu^{3+}$\$Tb^{3+}$ single-phase white-light-emitting phosphors. *J. Alloys Compd.*, 2020, **817**. 152687.

[15] Boatner L.A. Synthesis, structure, and properties of monazite, pretulite, and xenotime. *Phosphates: Geochemical, Geobiological and Materials Importance*, 2019, **48**, P. 87–122.

[16] Mesbah A., Clavier N., Elkaim E., Gausse C., Ben Kacem I., Szenknect S., Dacheux N. Monoclinic Form of the Rhabdophane Compounds: $REEPO_4 \cdot 0.667H_2O$. *Cryst. Growth Des.*, 2014, **14**, P. 5090–5098.

[17] Mesbah A., Clavier N., Elkaim E., Szenknect S., Dacheux N. In pursuit of the rhabdophane crystal structure: from the hydrated monoclinic $LnPO_4 \cdot 0.667H_2O$ to the hexagonal $LnPO_4$ (Ln = Nd, Sm, Gd, Eu and Dy). *J. Solid State Chem.*, 2017, **249**, P. 221–227.

[18] Duran E.C., Rafiuddin M.R., Shen Y., Hunt S.A., Mir A.H., Eggeman A.S. 3D electron diffraction studies of synthetic rhabdophane ($DyPO_4 \cdot nH_2O$). *Structural Chemistry*, 2024, **80** (10), P. 612–619.

[19] Osipov A.V., Mezentseva L.P., Drozdova I.A., Kuchaeva S.K., Ugolkov V.L., Gusarov V.V. Preparation and thermal transformations of nanocrystals in the $LaPO_4$–$LuPO_4$–H_2O system. *Glass Physics and Chemistry*, 2009, **35** (4), P. 431–435.

[20] Gavrichev K.S., Ryumin M.A., Tyurin A.V., Khoroshilov A.V., Mezentseva L.P., Osipov A.V., Ugolkov V.L., Gusarov V.V. Thermal behavior of $LaPO_4 \cdot nH_2O$ and $NdPO_4 \cdot nH_2O$ nanopowders. *J. of Thermal Analysis and Calorimetry*, 2010, **102**, P. 809–811.

[21] Luwang N., Ningthoujam R.S., Srivastava S.K., Vatsa R.K. Disappearance and Recovery of Luminescence in Bi^{3+}, Eu^{3+} Codoped YPO_4 Nanoparticles Due to the Presence of Water Molecules Up to 800 °C. *JACS*, 2011, **133**, P. 2998–3004.

[22] Awater R., Niemeijer-Berghuijsand L.C., Dorenbos P. Luminescence and charge carrier trapping in YPO_4:Bi. *Opt. Mater.*, 2017, **66**, P. 351–355.

[23] Yahiaoui Z., Hassairi M.A., Dammak M. Synthesis and Optical Spectroscopy of YPO_4:Eu^{3+} Orange-Red Phosphors. *J. Electron. Mater.*, 2017, **46**, P. 4765–4773.
[24] Chandrasekhar V., Metre R.K., Narayanan R.S. Lipophilic bismuth phosphates: A molecular tetradecanuclear cage and a 1D-coordination polymer. Synthesis, structure and conversion to $BiPO_4$. *Dalton Transactions*, 2013, **42** (24), P. 8709–8716.
[25] Zhao M., Li G., Zheng J., Li L., Wang H., Yang L. Preparation and polymorph-sensitive luminescence properties of $BiPO_4$:Eu, Part I: Room-temperature reaction followed by a heat treatment. *Cryst. Eng. Comm.*, 2011, **13**, P. 6251–6257.
[26] Wang R., Fan H., Ji Q., Imran M., Mujahid A., Wang J., Wang J., Zhang Y. Dressing Stark splitting of time-resolved excitation spectra in Eu^{3+}-doped $BiPO_4$ micro-crystals. *Optics and Laser Technology*, 2024, **176**, 110996
[27] Chang T.S., Guijia L., Shin C.H., Lee Y.K., Yun S.S. Catalytic behavior of $BiPO_4$ in the multicomponent bismuth phosphate system on the propylene ammoxidation. *Catal. Lett.*, 2000, **68**, P. 229–234.
[28] Ruwet M., Ceckiewicz S., Delmon B. Pure and Mo-Doped $BiPO_4$, Promoted by O_2, As a New Catalyst for Butyraldehyde Production. *Ind. Eng. Chem. Res*., 1987, **26**, P. 1981–1983.
[29] Iitaka K., Tani Y., Umezawa Y.Orthophosphate ion-sensors based on a quartz-crystal microbalance coated with insoluble orthophosphate salts. *Anal. Chim. Acta*, 1997, **338**, P. 77–87.
[30] Kalaiselvan S., Jeevanram R.K.A fast and simple method for the estimation of natural uranium in urine. *J. Radioanal. Nucl. Chem*., 1999, **240**, P. 277–279.
[31] Hölgye Z. Separation of neptunium from urine by coprecipitation with $BiPO_4$. *J. Radioanal. Nucl. Chem*., 1998, **227**, P. 127–128.
[32] Cheng L.W., Tsai J.C., Huang T.Y., Huang C. W., Unnikrishnan B., Lin Y.W. Controlled synthesis, characterization and photocatalytic activity of $BiPO_4$ nanostructures with different morphologies. *Materials Research Express*, 2014, **1** (2), 025023.
[33] Jermoumi T., Hafid M., Et-Tabirou M. Electrical conductivity study on Na_3PO_4-$Pb_3(PO_4)_2$-$BiPO_4$ phosphate glasses. *Mater. Sci. Eng. B*, 2001, **85**, P. 28–33.
[34] Elmoudane M., Et-Tabirou M., Hafid M. Glass-forming region in the system Li_3PO_4-$Pb_3(PO_4)_2$-$BiPO_4$(Li_2O-PbO-Bi_2O_3-P_2O_5) and its ionic conductivity. *Mater. Res. Bull*., 2000, **35**, P. 279–287.
[35] Zhao M., Li L., Zheng J., Yang L., Li G. Is $BiPO_4$ a better luminescent host? Case study on doping and annealing. *Inorg. Chem.*, 2013, **52**, P. 807–815.
[36] Gusarov V.V. Fast Solid-Phase Chemical Reactions. *Russ. J. Gen. Chem*., 1997,**67** (12), P. 1846–1851.
[37] Almjasheva O.V. The role of non-autonomous phases in the formation and transformation of solid-phase oxide systems. *Nanosystems: Phys. Chem. Math*., 2024, **15** (6), P. 755–767.
[38] Alexandrov A.A., Bragina A.G., Sorokin N.I., Voronov V.V., Luginina A.A., Kuznetsov S.V., Ivanov V.K., Fedorov P.P. Low-temperature phase formation in the BaF_2-LaF_3 system. *Inorganic Materials*, 2023, **59** (3), P. 295–305.
[39] Popkov V.I., Almjasheva O.V., Semenova A.S., Kellerman D., Nevedomskiy V., Gusarov V. Magnetic properties of $YFeO_3$ nanocrystals obtained by different soft-chemical methods. *J. Mater. Sci.: Materials in Electronics*, 2017, **28** (10), P. 7163–7170.
[40] Livage J. Quandl'air et l'eauremplacent le pétrole. *Le Monde*, 1977, 26 Octobre.
[41] Almjasheva O.V., Gusarov V.V. Metastable clusters and aggregative nucleation mechanism. *Nanosystems: Phys. Chem. Math*., 2014, **5** (3), P. 405–417
[42] Almjasheva O.V. Formation and structural transformations of nanoparticles in the TiO_2–H_2O system. *Nanosystems: Phys. Chem. Math*., 2016, **7** (6), P. 1031–1049.
[43] Almjasheva O.V., Denisova T.A. Water state in nanocrystals of zirconium dioxide prepared under hydrothermal conditions and its influence on structural transformations. *Russ. J. General Chemistry*, 2017, **87** (1), P. 1–7.
[44] Yan S.Q., Long C.G. Effects of Sm^{3+} concentration on the microstructure and luminescence properties of $BiPO_4$ phosphor prepared by hydrothermal method. *J. Mater. Sci.-Mater. Electron.*, 2016, **27**, P. 12079–12084.
[45] Xue F., Li H., Zhu Y., Xiong S., Zhang X., Tingting W., Liand X., Qian Y. Solvothermal synthesis and photoluminescence properties of $BiPO_4$ nano-cocoons and nanorods with different phases. *J. Solid State Chem*, 2009, **182**, P. 1396–1400.
[46] Proskurina O.V., Sivtsov E.V., Enikeeva M.O., Sirotkin A.A., AbievR.Sh., Gusarov V.V. Formation of rhabdophane-structured lanthanum orthophosphate nanoparticles in an impinging-jets microreactor and rheological properties of sols based on them. *Nanosyst.: Phys. Chem. Math.*, 2019, **10** (2), P. 206–214.
[47] Elovikov D.P., Osminina A.A. The role of the reaction medium pH in the formation of nanocrystalline phases in the Bi_2O_3–P_2O_5–H_2O system. *Nanosyst.: Phys. Chem. Math.*, 2024, **15** (3), P. 361–368.
[48] Enikeeva M.O., Kenges K.M., Proskurina O.V., Danilovich D.P., Gusarov V.V. Influence of Hydrothermal Treatment Conditions on the Formation of Lanthanum Orthophosphate Nanoparticles of Monazite Structure. *Russ. J. Appl. Chem*., 2020, **93**, P. 540–548.
[49] Enikeeva M.O., Yakovleva A.A., Proskurina O.V., Nevedomskiy V.N., Gusarov V.V. Phase formation under hydrothermal conditions and thermal transformations in the $GdPO_4$–YPO_4–H_2O system. *Inorg. Chem. Commun*., 2024, **159**, 111777.

Submitted 5 May 2025; accepted 18 June 2025

Information about the authors:

Alena A. Osminina – Branch of Petersburg Nuclear Physics Institute named by B. P. Konstantinov of National Research Centre "Kurchatov Institute" – Institute of Silicate Chemistry, 199034, St. Petersburg, Russia; Ioffe Institute, 194021, St. Petersburg, Russia; St. Petersburg State Institute of Technology, 190013, St. Petersburg, Russia; ORCID 0009-0008-8804-4732; alenaosminina3001@gmail.com

Dmitry P. Elovikov – Branch of Petersburg Nuclear Physics Institute named by B. P. Konstantinov of National Research Centre "Kurchatov Institute" – Institute of Silicate Chemistry, 199034, St. Petersburg, Russia; ORCID 0000-0003-4345-6086; syncdima@mail.ru

Olga V. Proskurina – Ioffe Institute, 194021, St. Petersburg, Russia; St. Petersburg State Institute of Technology, 190013,St. Petersburg, Russia; ORCID 0000-0002-2807-375X; proskurinaov@mail.ru

Conflict of interest: the authors declare no conflict of interest.